Atomic Hydrogen with Zirconium Halides in a Glow Discharge Plasma," *Vestn. Mosk. Univ. Khim.*, **16**, No. 1, 39 (1975).
Shelton, S. M., A. J. Kauffman, A. H. Roberson, E. D. Dilling, R. A. Beall, E. T. Hayes, H. Kato, J. H. McLain and F. Halbrook, "Zirconium—Its Production and Properties," *U. S. Bureau of Mines, Bulletin 561*, U. S. Government Printing Office, Washington, D. C. (1956).
Shen, J., and J. M. Smith, "Diffusional Effects in Gas-Solid Reactions," *Ind. Eng. Chem. Fundamentals*, **4**, No. 3, 293 (1965).
Sohn, H. Y., and J. Szekely, "A Structural Model for Gas-Solid Reactions with a Moving Boundary—III. A General Dimensionless Representation of the Irreversible Reaction Between a Porous Solid and a Reactant Gas," *Chem. Eng. Sci.*, **27**, 763 (1972).
Spink, D. R., "Extractive Metallurgy of Zirconium and Hafnium," *CIM Bulletin*, **70**, No. 787, 145 (1977).
Starrat, F. W., "Zirconium by Sodium Reduction," *J. Metals*, **11**, 441 (1959).
Stephens, W. W., and H. L. Gilbert, "Chlorination of Zirconium Oxide," *Trans. AIME, J. Metals*, **194**, 733 (1952).
Svehla, R. A., "Estimated Viscosities and Thermal Conductivities of Gases at High Temperatures," *NASA TR R-132* (1962).
Szekely, J., and J. W. Evans, "A Structural Model for Gas-Solid Reactions with a Moving Boundary," *Chem. Eng. Sci.*, **25**, 1091 (1970).
————., "A Structural Model for Gas-Solid Reactions with a Moving Boundary—II. The Effect of Grain Size, Porosity and Temperature on the Reaction of Porous Pellets," *ibid.*, **26**, 1901 (1971).
————., and H. Y. Sohn, *Gas-Solid Reactions*, Academic Press, New York (1976).
Tsirel'nikov, V. I., L. N. Kommissarova and V. I. Spitsyn, "Thermal Conductivity and Viscosity of Zirconium and Hafnium Tetrachloride Vapors at 300-700°," *Dokl. Akad. Nauk SSSR*, **139**, 1389 (1961).
Vasilenko, D. B., and A. N. Vol'skii, "The Thermodynamics of Reaction of Chlorination of Zirconium Dioxide by Gaseous Chlorine," *Russian J. Inorg. Chem.*, **3**, No. 7, 32 (1958).
Wang, S. C., and C. Y. Wen, "Experimental Evaluation of Nonisothermal Solid-Gas Reaction Model," *AIChE J.*, **18**, No. 6, 1231 (1972).
Wen, C. Y., "Noncatalytic Heterogenous Solid-Fluid Reaction Models," *Ind. Eng. Chem.*, **60**, No. 9, 34 (1968).
Wilke, C. R., "A Viscosity Equation for Gas Mixtures," *J. Chem. Phys.*, **18**, 157 (1950*b*).
Wilks, P. H., P. Ravinder, C. L. Grant, P. A. Pelton, R. R. J. Downe and M. C. Talbot, "Plasma Process for Zirconium Dioxide," *Chem. Eng. Progr.*, **68**, 82 (1972).
Wilks, P. H., P. Ravinder, C. L. Grant, P. A. Pelton, R. R. J. Downe and M. C. Talbot, "Commercial Production of Submicron Zirconium Dioxide via Plasma," *Chem. Eng. World*, 9, (3), Section 1, 59 (1974).
Williams, R. J. J., A. Calvelo and R. E. Cunningham, "A General Asymptotic Analytical Solution for Non-Catalytic Gas-Solid Reactions," *Can. J. Chem. Eng.*, **50**, 486 (1972).
Yagi, S., and D. Kunii, "Proposed Theory of Fluidized Roasting of Sulfide Ore with Uniform Size. I—Single Particle of Ore in the Fluidized Bed," *J. Chem. Soc. Japan, Ind. Chem. Sect.*, **56**, 131 (1953).
Yagi, S., and D. Kunii, "Fluidized-Solid Reactors for Particles with Decreasing Diameters," *Chem. Eng. Japan.*, **19**, 500 (1955*a*).
————., "Combustion of Carbon Particles in Flames and Fluidized Beds," *Symposium on Combustion*, 5th, Pittsburgh, 1954, Reinhold, New York, 231 (1955*b*).

Manuscript received August 3, 1979; revision received February 21, and accepted February 29, 1980.

Simultaneous Melting and Freezing in the Impingement Region of a Liquid Jet

MICHAEL EPSTEIN
M. J. SWEDISH
J. H. LINEHAN
G. A. LAMBERT
G. M. HAUSER
and
L. J. STACHYRA

Reactor Analysis and Safety Division
Argonne National Laboratory
9700 South Cass Avenue
Argonne, Illinois 60439

An experimental investigation of an impinging water jet freezing on a melting solid surface has been carried out. Attention was focused on the stagnation region of an axisymmetric jet. In the experiment, a water jet was directed upward against the lower end of a meltable rod, having a diameter about twice that of the jet orifice. Solid octane (m.p.—56.5°C) and solid mercury (m.p.—38.9°C) served as the meltable materials. A laminar-axisymmetric flow model was developed to describe melting heat transfer in the presence of jet solidification within the impingement region. Measurements of the melting rate and conditions for the onset of jet solidification were found to agree quite well with the values predicted with this model.

SCOPE

There is extensive literature on fluid convection problems involving phase changes that pertain to either a warm liquid flowing over a melting surface or the solidification of a molten stream on a cooled wall. However, this mutually exclusive situation is not always the case. If the molten stream and the wall are different materials of immiscible liquids, with the fusion temperature of the hot flowing material exceeding that of the wall material, melting of the wall and freezing of the flow can take place simultaneously. An example, which is important to fast reactor safety research, is the melting of solid steel (m.p. 1 410°C) immersed in a flow of molten ceramic UO_2 (m.p. 2 850°C). An important conclusion arising out of past theoretical and experimental work on this problem is that the steel melting rate is controlled by a frozen layer (or crust) of UO_2 which floats on the steel melt.

An investigation of frozen crust behavior which yielded results of qualitative interest for our present purposes is that of Epstein (1977). In this work, a linear stability analysis was employed to study the mechanical behavior of a growing crust on an underlying lighter melt layer in a gravity field. The analysis compared well with experimental observations for low melting material pairs. A notable result was that a ceramic UO_2 crust growing on melting steel was predicted to be stable against buoyancy forces. Further evidence for the existence of a protective crust has been found by injecting hot Freon 112A

J. H. Linehan is at Marquette University, Milwaukee, Wisconsin.

0001-1541-80-3903-0743-$01.05.

(m.p. 40°C) into a thick walled ice pipe maintained at its melting temperature throughout (Yim et al., 1978). The major emphasis in this study was on the melting attack of the ice pipe wall by the turbulently flowing Freon. Sections of freon crust were observed to form on the inner melting ice wall and slide over the melting ice with a jerking motion in the direction of flow. Numerical results based on a stable freon-crust/ice-melt film model were compared with the experimentally determined results for ice melting. Despite the complex crust motion and the absence of a continuous crust surface, the model was found to represent the data reasonably well.

The objective of the work reported here was to investigate simultaneous melting and freezing in the impingement region of a liquid jet. The integrity of protective steel barriers when subjected to jets of molten ceramic fuel is an important safety question in current design of in-pile experiments that attempt to simulate postulated core disruptive accidents for the fast breeder reactor. Accordingly, the present experimental study deals with a liquid jet impinging and freezing on a melting solid surface. Attention was focused on the stagnation region of an axisymmetric jet. As in a recent investigation of impingement heat transfer with melting only (Swedish et al., 1979), a water jet was directed upward against the lower end of a meltable solid rod having a diameter about twice that of the jet orifice. In the experiments reported here, however, our choice of meltable rod materials resulted in simultaneous freezing of the water jet and melting of the solid rod. Solid octane (m.p.—56.5°C) and solid mercury (m.p.—38.9°C) served as the meltable solid materials.

A simple model of this dual phase conversion process was developed to describe melting heat transfer in the presence of jet solidification and to accurately predict the threshold jet temperature for incipient jet solidification. In this model, the liquid melt (layer) that formed at the melting surface was assumed to be separated from the oncoming liquid jet by a stationary crust of frozen jet material. The motion of the melt layer was assumed axisymmetric and driven by the pressure (or force) exerted by jet impingement on the opposite surface of the crust.

Previous studies considering liquid-solid phase change at a stagnation point by Roberts (1958), Yang (1966), Savino et al. (1970), Yen and Zehnder (1973), Gilpin (1973), Yen (1975), Lipsett and Gilpin (1978), and Swedish et al. (1979) have been limited to either liquid jet solidification or melting of the impingement surface. There have been no prior investigations of simultaneous liquid jet solidification and melting of the impingement surface.

CONCLUSIONS AND SIGNIFICANCE

When a hot molten jet is directed against a low, melting point solid of a different material, simultaneous freezing of the jet and melting of the solid can occur. A detailed study of this process has been made utilizing a water jet directed against a solid octane or solid mercury surface. In accordance with results from other flow systems with simultaneous melting and freezing (Epstein, 1977; Yim et al., 1979), it was found that the melting rate of the solid was controlled by a frozen crust of jet material that separates that liquid formed by melting from the hot molten stream. The following observations were made that lend support to this conclusion:

1. The melting rate of the solid was found to be a function of the difference between the liquid jet temperature and the freezing temperature of the jet material. That is, the melting rate of the solid tends toward zero as the temperature of the impinging jet approached its freezing temperature.
2. Experimentally observed melting rates were in good agreement with the predictions of a simple axisymmetric melt flow model. In this model it was proposed that a stable circular disk of ice separates the impinging water jet from the melt layer and causes the melt to be expelled radially from between the melting surface and the ice crust.
3. A step reduction in the melting rate of octane was observed as the water jet was cooled below 13°C. This discontinuity in the melting rate was found to be insensitive to variations in jet velocity and was accurately predicted by the model to be the temperature for incipient ice crust formation.
4. When the water jet temperature was reduced below about 5°C, the circular (disk) ice crust at the melting surface was readily observed.

PHYSICAL MODEL

A schematic representation of the physical model and coordinate system is shown in Figure 1. A round jet of hot liquid at a velocity w_∞ and temperature T_∞ above its solidification temperature T_{mp} impinges on the circular end of a solid (rod) of different material. Initially, the temperature of the solid is at T_0 below its melting temperature $T_{mp,s}(T_{mp} > T_{mp,s} > T_0)$. Upon contact, the temperature of the interface separating the molten jet and the solid falls between T_{mp} and $T_{mp,s}$ resulting in solidification in the liquid jet and melting of the solid. A layer of frozen jet material (crust) is assumed to build up on the underlying melting surface. After a short initial period, during which the crust and melt layer grow at rates determined by transient heat conduction, the crust stops growing and divides the flow field into two separate, steady state flow regions, as sketched in Figure 1. Of course, in order to achieve steady state conditions, the melt film has to be expelled in the radial direction r by the jet thrust on the opposite side of the crust working against the viscous resistance and inertia of the melt film.

The assumption of a frozen layer of jet material that isolates the surface melt from the impinging jet seems reasonable when one considers that the hot jet contacts an initially cold, solid surface. Crust growth and melting of the solid substrate begin simultaneously. Because of the thrust exerted by the jet on the crust, the rate of removal of melt material in the radial direction is high, and the melt layer remains thin. Thus, the possibility of mixing between molten jet and melt material, which would be expected to interfere with the development of a frozen layer of jet material, seems unlikely. In addition, according to the analysis of Erickson and Olfe (1978), an instability of the Kelvin-Helmholtz type (at the liquid jet melt film interface in the absence of an intervening crust) is bounded in the stagnation counterflow illustrated in Figure 1. Thus, even if the jet impinges on a pre-existing melt layer at time $t = 0$, a molten jet melted substrate mixing zone will probably fail to materialize. Moreover, in our experiments a stationary disk of frozen jet material protecting the melting surface was visually observable when the jet temperature was sufficiently low (see below).

In addition to the foregoing considerations of jet solidification, the following assumptions are made:

A1. The initial transient conduction stage discussed above is ignored, and we assume the melting process to occur under

steady state conditions. The melt thickness δ and the crust thickness δ_c are constant in time. The relaxation time to steady state in the melting solid is easily seen to be comparable to the time it takes the thermal wave thickness $(\alpha_s t)^{\frac{1}{2}}$ to span one steady state boundary layer thickness, α_s/V_m, namely, $t \sim \alpha_s/V_m^2$. Similarly, the transient in the melt layer will die out in about the time it takes the thermal conduction wave thickness $(\alpha_m t)^{\frac{1}{2}}$ to traverse δ; namely, $t \sim \delta^2/\alpha_m$. [Low Prandtl number melt layers require the momentum wave thickness $(\nu_m t)^{\frac{1}{2}}$ to span δ or $t \sim \delta^2/\nu_m$ to ensure steady state.] The crust will grow to its steady state thickness after a time $t \sim \delta_c^2/\alpha_c$. From the results of the analysis, we find that for most material pairs of practical interest (including the UO_2-steel system), the relaxation time for attainment of steady state is less than 0.1 s, which is completely negligible on the time scale of the experiment (see below). The coordinate system chosen is fixed to the melting surface. In this coordinate system, the interior of the melting solid moves toward the stationary crust with constant velocity equal to the melting velocity, as in the experimental technique described below.

A2. The present analysis is restricted to the neighborhood of the stagnation point of the axisymmetric external jet flow. According to measurements made with gas jets, the axisymmetric stagnation flow model breaks down at a radial distance of about 1.2 times the jet (or nozzle) diameter d (see Martin, 1977, for a summary of this work). The crust disk, whose maximum radial extent is $r = R$, is assumed to lie entirely within this stagnation zone.

A3. Under steady state conditions, the melt flow moves radially outward between the crust and the melting surface. The observation of a stationary crust disk and considerations of symmetry would suggest an axisymmetric flow in the melt layer. Because of a low calculated Reynolds number, the melt flow is assumed laminar. Exit effects at the radial location $r \simeq R$ where the melt layer emerges from between the melting surface and the crust disk are neglected. This assumption is valid as long as the melt film thickness and the thermal boundary layer thickness in the melting solid are small compared with the radius of the crust disk (that is, $\delta/R \ll 1.0$).

A4. Because of the presence of the stationary protective crust, the liquid velocities at the upper and lower crust surfaces are set equal to zero. Therefore, the upper crust surface acts as a solid wall as far as the oncoming molten jet is concerned. Also, since the crust molten jet interface is at the fusion temperature of the jet material T_{mp}, motion and heat convection within the jet are not affected by the presence of the underlying melt layer.

A5. The thicknesses of the melt layer and the crust are assumed to be spatially uniform. From stagnation flow theory, it is known that both the boundary layer thickness and the rate of heat transfer from the jet in the downward direction are independent of the radial distance r. Thus, we anticipate that the crust and melt layer have uniform thicknesses.

A6. The protective crust disk is assumed to be rigid. The normal force exerted on the upper surface of the crust is obtained by integrating the potential flow pressure distribution for the external liquid jet motion. Since the crust is stationary, the melt film must exert an opposing force of identical magnitude on the lower crust surface which is derived from the integral of the pressure distribution within the flowing melt. In this force balance (of vertical forces), we neglect the mass of the crust which can be shown to be negligible.

A7. All physical properties are considered constant. The properties of the melt layer are evaluated at the average melt film temperature $\frac{1}{2}(T_i + T_{mp,s})$. The properties of the jet flow field are evaluated at $\frac{1}{2}(T_\infty + T_{mp})$. In addition, the densities of liquid melt and solid substrate are assumed to be approximately equal.

We might remark that the axisymmetric flow model depicted in Figure 1 is not without precedent. A similar model has been used by Roberts (1958) and more recently by Swedish et al. (1979) to predict melting rates in the jet impingement region in the absence of jet solidification. In the latter study, the theoretical predictions were found to be in good agreement with experimental results. A closely related problem, as far as the motion of the melt layer is concerned, arises in the study of the squeeze film. In this application, an axisymmetric film flow is treated in a quasi steady manner to obtain the rate of thinning of liquid or gaseous films trapped between two rigid parallel disks being forced together (see, for example, Charles and Mason, 1960).

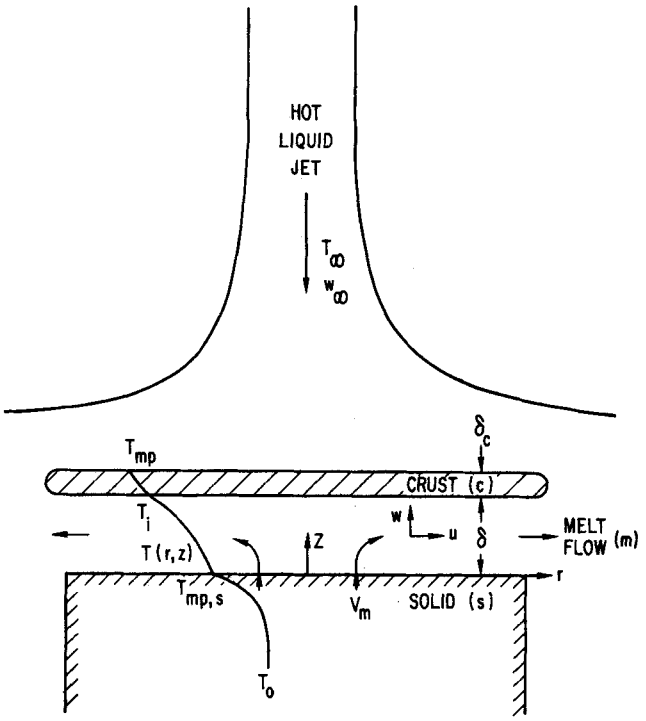

Figure 1. Schematic diagram of a stationary crust embedded in an axisymmetric stagnation flow; indicating temperature profile and nomenclature.

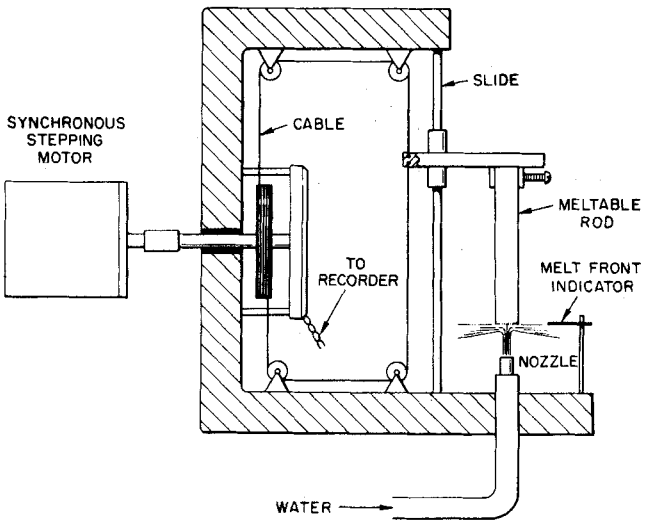

Figure 2. Schematic diagram of the experimental apparatus.

ANALYSIS

It is convenient to begin the analysis by separate considerations of the jet region and the melt layer.

Jet Region

According to our model, the flow field above the crust satisfies the governing equations for axisymmetric stagnation flow. In the

neighborhood of the stagnation point, the heat flux q through the upper surface of the crust is given by

$$q = k(T_\infty - T_{mp})\sqrt{\frac{2a}{\nu}}\,\theta'(0) \tag{1}$$

The dimensionless temperature gradient $\theta'(0)$ at the upper crust surface is a function of the Prandtl number Pr of the liquid jet. Calculations performed by Stewart and Prober (1962) suggest that this function can be approximated for $Pr > 0.5$ by $\theta'(0) = 0.55\ Pr^{0.35}$. In the above expression a is the stagnation point velocity gradient. It has been found experimentally that $a \simeq w_\infty/d$, where d is the diameter of the nozzle from which the jet emerges (Martin, 1977). Strictly speaking, Equation (1) is only valid for laminar stagnation flow. Available data and analysis for turbulent air jets suggest that for impingement close to the stagnation point, the heat (or mass) transfer can be computed by applying turbulent correction factors to the laminar values (Donaldson et al., 1971; Giralt et al., 1977). The correction factors have been found to be only a function of the axial nozzle orifice to impingement surface distance and not a function of jet Reynolds number. For nozzle to surface distances less than 4 nozzle diameters, it was concluded that significant penetration of turbulence into the boundary layer near the surface does not occur, as there is good agreement between laminar predictions and measured rates. For larger axial distances, turbulence in the impinging jet is high, and laminar predictions fall below measured values. This behavior leads one to suspect that the initial nozzle induced turbulence does not affect the rate of heat transfer, but, instead, it is the interaction of the air jet with the surrounding atmosphere that causes the increased heat transfer rates. In view of this and the fact that the interaction between a liquid jet and its surrounding air atmosphere is so much less than that for an air jet, it is unlikely that the turbulence correction factor is required for a liquid jet. Available heat transfer data for liquid jets (Sitharamayya and Subba Raju, 1969; Swedish et al., 1979) indeed indicate that (1) can be successfully applied when the jet is turbulent.

The pressure distribution at the upper surface of the crust is the same as if the jet flow is ideal, namely

$$P = p_0 - \frac{1}{2}\rho a^2 r^2 \tag{2}$$

Melt Layer Region

In view of assumptions A1 and A3, the flow field in the melt layer is taken to correspond to steady, laminar axisymmetric flow. Accordingly, the velocity field must satisfy the partial differential equations

$$u\frac{\partial u}{\partial r} + w\frac{\partial u}{\partial z} = -\frac{1}{\rho_m}\frac{\partial p}{\partial r} + V_m\left(\frac{\partial^2 u}{\partial r^2} + \frac{1}{r}\frac{\partial u}{\partial r} - \frac{u}{r^2} + \frac{\partial^2 u}{\partial z^2}\right) \tag{3}$$

$$u\frac{\partial w}{\partial r} + w\frac{\partial w}{\partial z} = -\frac{1}{\rho_m}\frac{\partial p}{\partial z} + \nu_m\left(\frac{\partial^2 w}{\partial r^2} + \frac{1}{r}\frac{\partial w}{\partial r} + \frac{\partial^2 w}{\partial z^2}\right) \tag{4}$$

$$\frac{\partial u}{\partial r} + \frac{u}{r} + \frac{\partial w}{\partial z} = 0 \tag{5}$$

while the temperature field must satisfy

$$u\frac{\partial T}{\partial r} + w\frac{\partial T}{\partial z} = \alpha_m\left(\frac{\partial^2 T}{\partial r^2} + \frac{1}{r}\frac{\partial T}{\partial r} + \frac{\partial^2 T}{\partial z^2}\right) \tag{6}$$

The boundary conditions are (see assumptions A4 and A5 and Figure 1)

$$\text{at } z = 0\text{: } u = 0,\ w = V_m \text{ (melting velocity)},\ T = T_{mp,s} \tag{7}$$

$$\text{at } z = \delta\text{: } u = 0,\ w = 0,\ T = T_i \tag{8}$$

$$\text{at } r = 0\text{: } u = 0 \tag{9}$$

$$\text{at } r = 0,\ z = \delta\text{: } p = p_0 \tag{10}$$

The value of T_i is not known a priori; rather it must be determined as part of the solution.

Compatibility Conditions

The heat flux from the melt film to the melting solid must supply sufficient heat to raise the solid temperature from its initial value T_0 to its melting temperature $T_{mp,s}$ and to supply the latent heat of melting L. It can be shown that this condition takes the form (Carslaw and Jaeger, 1959)

$$k_m\left(\frac{\partial T}{\partial z}\right)_{z=0} = [L + c_s(T_{mp,s} - T_0)]\rho_m V_m \tag{11}$$

The heat flux is continuous through the frozen layer

$$k_m\left(\frac{\partial T}{\partial z}\right)_{z=\delta} = \frac{k_c(T_{mp} - T_i)}{\delta_c} = q \tag{12}$$

A mechanical force balance applied to the crust requires that (see Assumption A6)

$$\int_0^R P(r)\,2\pi r\,dr = \int_0^R p(r,\delta)\,2\pi r\,dr \tag{13}$$

Similarity Transformaton for the Melt Layer

A similarity transformation can be effected by recognizing that the governing equations and boundary conditions between the three-dimensional (axisymmetric) stagnation flow problem and the present melt layer flow problem are similar. The transforms for the stagnation flow problem are assumed (Schlichting, 1960):

$$\eta = (2a_m/\nu_m)z^{1/2},\ u = a_m r f'(\eta),\ w = -(2a_m\nu_m)^{1/2} f(\eta) \tag{14}$$

$$p(r,\eta) = -\frac{1}{2}\rho_m a_m^2[r^2 + (\nu_m/a_m)F(\eta)] \tag{15}$$

$$\phi = \frac{T(\eta) - T_{mp,s}}{T_i - T_{mp,s}} \tag{16}$$

These transformations satisfy the requirements of reducing the partial differential Equations (3) to (6) into ordinary differential equations and of satisfying the radial boundary condition of Equation (9). An important consequence of the radial independence of T is that the melting rate V_m and the interface T_i are independent of r. The applicability of the transforms for stagnation flow to melting problems of this class has been discussed in some detail by Roberts (1958). The stagnation point velocity gradient for the melt layer a_m that appears in Equations (14) and (15) is a constant of proportionality (to be determined).

Substituting Equations (14) to (16) into Equations (3) to (6) yields*

$$f''' + ff'' + \frac{1}{2}(1 - f'^2) = 0,\ F' = 4(ff' + f'') \tag{17}$$

$$\phi'' + Pr_m f\phi' = 0 \tag{18}$$

The primes denote differentiation with respect to η. The boundary conditions (7) and (8) become

$$\text{at } \eta = 0\text{: } f' = 0,\ f = -V_m/(2a_m\nu_m)^{1/2},\ \phi = 0 \tag{19}$$

$$\text{at } \eta = \eta_\delta\text{: } f' = 0,\ f = 0,\ \phi = 1.0 \tag{20}$$

Evaluating Equation (15) at the lower surface of the crust, one obtains

*Note that it is not necessary to evaluate the function $F(\eta)$ unless the pressure distribution within the melt flow field is required.

$$p(r, \eta_\delta) = p_0 - \frac{1}{2}\rho_m a_m^2 r^2 \tag{21}$$

Substituting equations (2) and (21) into the force balance (13), we get†

$$\rho a^2 = \rho_m a_m^2 \tag{22}$$

From Equations (1), (11), (12) and (22), it can be shown that the dimensionless group $f(0)\phi'(\eta_\delta)/\phi'(0)$ can be replaced by another dimensionless group which contains physical quantities which would be known in any physical situation, namely

$$N \equiv A \cdot B \cdot \frac{k}{k_m} \cdot \theta'(0) = -\frac{f(0)\phi'(\eta_\delta)}{\phi'(0)} Pr_m \tag{23}$$

where

$$B \equiv \frac{c_m(T_\infty - T_{mp})}{L + c_s(T_{mp,s} - T_0)}, \quad A = \sqrt{\frac{\nu_m}{\nu}\left(\frac{\rho_m}{\rho}\right)^{1/2}} \tag{24}$$

For a fixed Pr_m, Equation (23) provides a unique relation between the melt layer thickness η_δ and N. As soon as solutions are available as a function of η_δ, corresponding values of N can be computed from this expression. Consequently, the present problem in fact involves only two dimensionless physical parameters, Pr_m and N.

Melting Velocity, Interface Temperature and Crust Thickness

In the preceding sections, the governing differential equations for the velocity and temperature distributions have been derived. Here the solutions of these equations are related to quantities of practical interest. From Equations (19), (22) and (23), the expression for the melting velocity V_m becomes

$$\frac{V_m}{\alpha_m(2a/\nu)^{1/2}} = \frac{\phi'(0)}{\phi'(\eta_\delta)} \cdot \frac{k}{k_m} \cdot B \cdot \theta'(0) \tag{25}$$

Substituting Equations (1) and (14) into Equation (12), we obtain

$$\frac{T_i - T_{mp,s}}{T_\infty - T_{mp}} = \frac{\theta'(0)}{\phi'(\eta_\delta)} \cdot \frac{k}{k_m} \cdot A \tag{26}$$

for the temperature at the lower crust surface and

$$\left(\frac{2a}{\nu}\right)^{1/2} \cdot \delta_c = \frac{k_c}{k} \cdot \frac{T_{mp} - T_i}{T_\infty - T_{mp}} \cdot \frac{1}{\theta'(0)} \tag{27}$$

for the thickness of the protective crust. It is seen from Equations (25) to (27) that once the dimensionless temperature gradients $\phi'(0)$ and $\phi'(\eta_\delta)$ have been supplied by the solutions of Equations (17) and (18), then the quantities V_m, T_i and δ_c are immediately known.

Incipient Crust Formation

If the jet temperature T_∞ is too high, crust formation will not occur. The critical jet temperature above which crust formation will not take place, $T_{\infty,\text{crit}}$, is obtained by setting $T_i = T_{mp}$ in Equation (26):

$$\frac{T_{\infty,\text{crit}} - T_{mp}}{T_{mp} - T_{mp,s}} = \frac{\phi'(\eta_\delta)}{\theta'(0)} \cdot \frac{k_m}{k} \cdot \frac{1}{A} \tag{28}$$

By eliminating $T_{\infty,\text{crit}}$ between Equations (23) and (28), we find that, at incipient crusting, Equation (23) is replaced by

$$\frac{c_m(T_{mp} - T_{mp,s})}{L + c_s(T_{mp,s} - T_0)} = -\frac{f(0)}{\phi'(0)} \cdot Pr_m \tag{29}$$

Thin Melt Film Solution

When the liquid melt film is very thin, the melt film Reynolds and Peclet numbers are small so that the inertia terms in the momentum equation and the convection term in the energy equation can be neglected (creeping flow). In the absence of inertia and convection terms, Equations (17) and (18) become

$$f''' = -\frac{1}{2}, \quad \phi'' = 0 \tag{30}$$

The solution of these equations which satisfy boundary conditions (19) and (20) are

$$f = -\frac{1}{12}\eta^3 + \frac{1}{8}\eta_\delta\eta^2 + f(0), \quad \phi = \frac{\eta}{\eta_\delta} \tag{31}$$

where

$$f(0) = -\frac{1}{24}\eta_\delta{}^3 \tag{32}$$

From Equations (23) and (32), we obtain the melt layer thickness

$$\eta_\delta = \left(\frac{24N}{Pr_m}\right)^{1/3} \tag{33}$$

All other quantities of interest follow immediately from Equations (25) to (29):

$$\sqrt{\frac{\nu_m}{2a}\left(\frac{\rho_m}{\rho}\right)^{1/2}} \cdot \frac{V_m}{\alpha_m} = N \tag{34}$$

$$\frac{T_i - T_{mp,s}}{T_\infty - T_{mp}} = \theta'(0) \cdot \frac{k}{k_m} \cdot A \cdot \left(\frac{24N}{Pr_m}\right)^{1/3} \tag{35}$$

$$\frac{T_{\infty,\text{crit}} - T_{mp}}{T_{mp} - T_{mp,s}} = \frac{k_m}{k} \cdot \frac{1}{A\theta'(0)} \cdot \left[\frac{Pr_m}{24} \cdot \frac{L + c_s(T_{mp,s} - T_0)}{c_m(T_{mp} - T_{mp,s})}\right]^{1/4} \tag{36}$$

Equations (35) and (36) indicate that the temperature of the lower surface of the crust and the threshold jet temperature for crust formation are independent of the jet velocity w_∞. The latter result is borne out by the experiments with the water jet and octane rod (see below).

Numerical Solution

When inertia and convective terms are retained, we must deal with Equations (17) and (18). Numerical solutions of these equations were obtained for liquid melt film Prandtl numbers between 0.001 and 100.0 and for N ranging from essentially 0 to 100.0. Figures presenting the jet temperature at incipient crust formation $T_{\infty,\text{crit}}$, the temperature at the lower surface of the crust T_i and the melt layer thickness δ are presented elsewhere (Epstein et al., 1978).

The computation of melting rates, interface temperature, etc., should begin with the evaluation of $T_{\infty,\text{crit}}$ to determine whether or not a protective crust of jet material will form for the particular pair of materials and jet temperature of interest.

APPARATUS AND EXPERIMENTAL TECHNIQUE

The experimental apparatus and procedures used were essentially the same as those described by Swedish et al. (1979). There were, however, a few modifications in order to accommodate a solid mercury substrate.

The experimental apparatus is shown in Figure 2. Water from a large constant-temperature reservoir is passed through a nozzle. The water jet is directed upward against the lower end of a meltable rod, having a diameter about twice that of the nozzle. The selection of the diameters of the nozzle and the impingement surface was made to ensure that a flat melting surface was maintained, so that melting rate measurements were indeed restricted to the stagnation region. The meltable rod is attached to a slide so that its vertical position is adjustable through the action of a high tension cable. The movement of the cable was controlled with a variable speed electric motor. The jet is deflected by the melting impingement surface, thereby setting up a flow of liquid normal to the jet that spreads radially outwards and forms a free fan jet a short distance from the edge of the melting surface. A thin plate, which serves as a melt front finder (or indicator), is located a fixed distance above the base of the apparatus by means of a support pin. During a run, the melting rod was

†This implies that $P(r)$ in the jet equals $p(r, \delta)$ in the melt region. Recall that we have ignored the mass of the crust in arriving at this result. Interestingly enough, Equation (22) can be shown to apply even if the mass of the crust is included in the analysis.

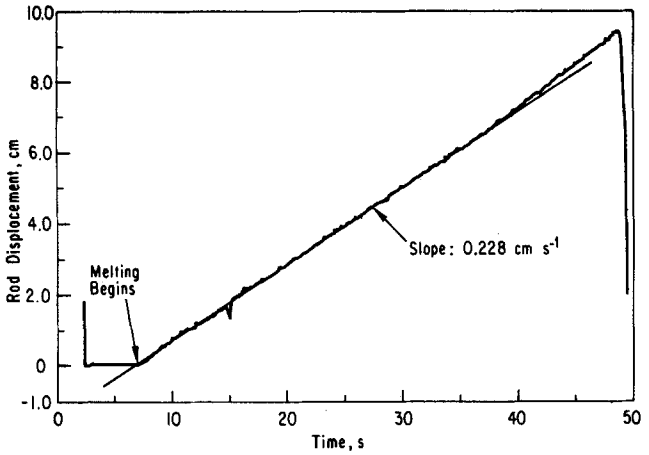

Figure 3. Typical record of octane rod displacement. Jet velocity, 1.39 m s^{-1}; jet temperature, 20°C.

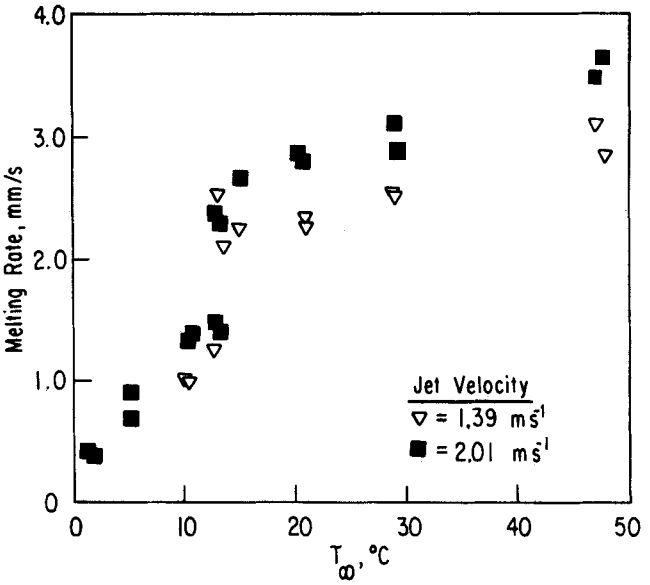

Figure 4. Melting rate of octane rod as a function of jet temperature; jet velocity as a parameter.

fed into the jet at a rate such that the indicator plate remained submerged in the thin fan jet deflected by the melting surface. This measure proved to be fully successful in achieving a constant separation distance between the nozzle and the melting surface.* The rod melting rates were determined with the aid of instrumentation which converts the downward rod displacement history into an electric signal that can be read and recorded on an electronic strip chart recorder. Figure 3 is a copy of a typical chart record showing the rod displacement as a function of time for water impinging on a melting octane rod.

The test specimens were cylindrical rods of frozen octane (m.p. −56.6°C) and frozen mercury (m.p. −38.9°C) about 15 cm high and 0.95 cm in diameter. The casting of the octane rods was accomplished in a copper tube mold (described by Swedish et al., 1979). The octane was frozen in a liquid nitrogen bath (−196°C). The casting of the mercury rods was carried out in glass molds. In essence, each mold resembled a test tube with a flat bottom. The liquid mercury was poured into the glass tube, and the tube was plugged at the top with a threaded teflon fitting. The fitting was used in handling the rod and for attaching it to the adjustable slide. As with the octane rods, the mercury was frozen in a liquid nitrogen bath. Unmolding of the solidified mercury rod was accomplished by strategic hammer blows that caused the glass mold to shatter.

A number of precautions were taken in the design and conduct of the experiments to control the mercury inventory and ensure that the room was free of mercury vapor. The nozzle, the melt front indicator and the mercury rod were all housed within a cylindrical Lucite container (not shown in Figure 2). The nozzle tube is inserted through the center of the bottom of the Lucite container with the nozzle about 4.2 cm above the bottom. When the jet is turned on, a pool of water forms at the bottom of the container. Three drains are installed in the walls of the container to prevent the water pool from covering the nozzle. With this design, during a run, the melted mercury falls to the bottom of the container and remains submerged in the water pool formed by the deflected jet. In addition, the jet velocities were restricted to 200 cm s^{-1} when the jet temperature exceeded 40°C to prevent the liquid mercury from being swept out the top of the container. An outside exhaust system was used while the mercury (or octane) experiments were in progress.

Before an experimental run was made, the meltable rod was removed from the liquid nitrogen bath, mounted on the apparatus and allowed to warm by convection in the air. The purpose of this warm-up period was to reduce the effect of rod subcooling on measured melting rates. Preliminary tests, in which the temperature of the center of the rod was monitored as it was removed from the liquid nitrogen and placed in the fixture, showed that a minimum of about 2.5 min was required to eliminate most of the subcooling. Thus, in comparing the above analysis with the data, the quantity $c_s(T_{mp,s} - T_0)/L$, which governs the importance of rod heat capacity effects, can be neglected.

All the data reported here were obtained at a nozzle-to-rod spacing of 2.38 cm. The nozzle had a diameter of 4.76 mm. The effects of nozzle-to-rod distance and nozzle design on rod melting rates were found to be insignificant (Swedish et al., 1979). The rod melting experiments covered water jet velocities (mean nozzle velocities) from 1.66 to 3.16 m s^{-1} and jet temperatures ranging from 1.0° to 80°C.

* Note that the melting surface in the experiment is upside down in relation to that shown in the schematic of the physical model (Figure 1).

EXPERIMENTAL RESULTS AND DISCUSSION

For a given jet velocity, there are two sharply defined melting regimes for the water-jet/octane-rod system. This is illustrated

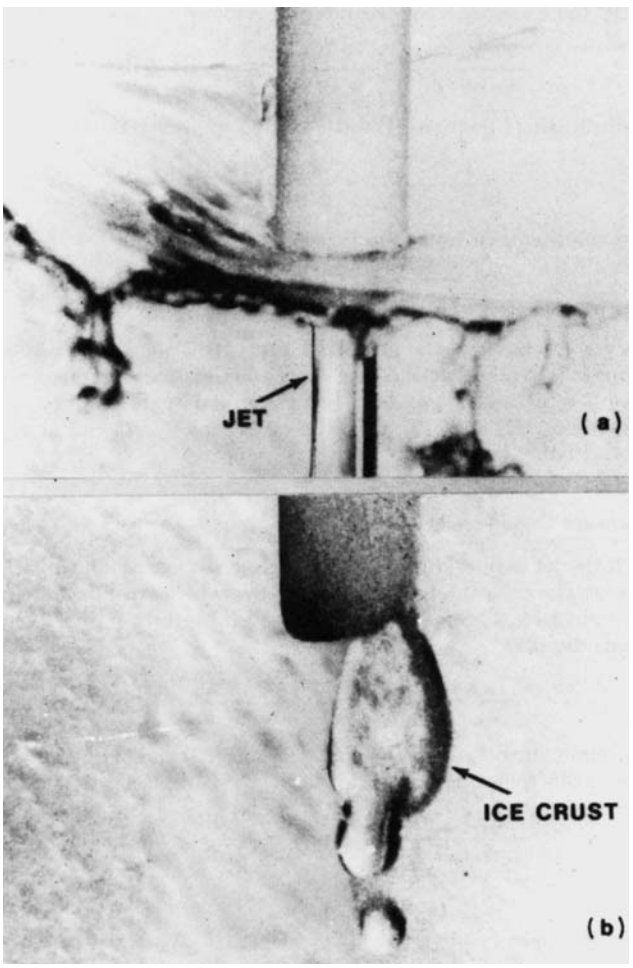

Figure 5. *a*. Water jet impingement on the lower end of a melting octane rod.
***b*. Ice crust separating from octane rod immediately after the jet is shut off. Note the liquid octane film developing into a drop at the lower end of the falling ice disk.**

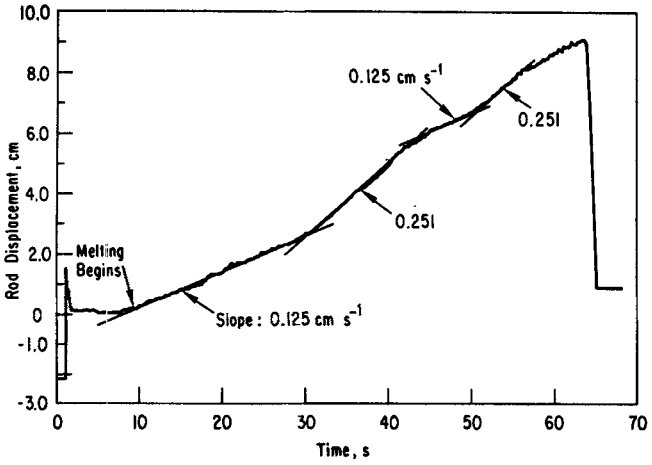

Figure 6. Chart of octane rod displacement vs. time, s. Jet velocity, 1.39 m s^{-1}; jet temperature, 13°C.

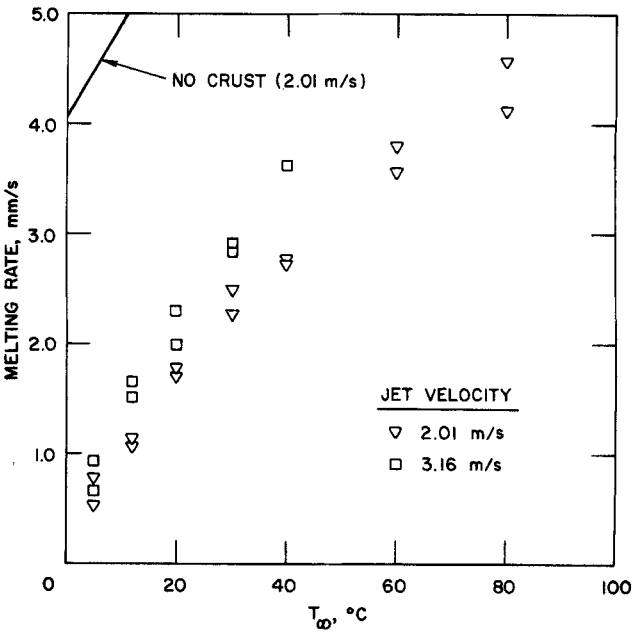

Figure 7. Melting rate of mercury rod as a function of jet temperature; jet velocity as a parameter.

in Figure 4, which shows a typical plot of melting velocity of an octane rod against water jet temperature. The melting rate data fall on two different curves depending on whether the jet temperature is less than or greater than 13°C. For jet temperatures in the range $0 < T_\infty < 13$°C, the melting velocity increases rapidly with increasing jet temperature, whereas for $T_\infty > 13$°C, the melting velocity is relatively insensitive to the jet temperature. This behavior is believed to be directly related to the formation of a protective ice crust on the octane melt layer when the jet temperature falls below 13°C, as manifest by the step change in rod melting rate. If heat is transferred from the liquid jet to the octane melt front through a layer of ice, which isolates the melting octane from the water jet, the heat flux is proportional to the difference between the jet temperature and the ice melting temperature. Therefore, we expect the melting rate to fall off rapidly as the jet temperature decreases and tend to zero when $T_\infty \to 0$°C.* This behavior is clearly seen in Figure 4. On the other hand, beyond the point of incipient crust formation when $T_\infty > 13$°C, the thermally protective ice crust is absent. The melting octane is directly exposed to the hot water jet, and the relevant temperature difference for heat convection is the jet temperature minus the octane melting temperature (−56.5°C). Thus, the convective flux can only vary by at most 50% over the jet temperature range 14° to 50°C.

Experiments carried out with the water-jet/octane-rod system at increased jet velocities of 2.80 and 3.16 m s^{-1} also revealed the step change behavior shown in Figure 4 when T_∞ was about 13°C. This threshold was reproducible to within ±1.0°C. The jet temperature required for a step change in melting rate appears to be insensitive to jet velocity. Thus, this step change is not likely due to a change in flow pattern such as a transition from laminar to turbulent flow in the impingement region. Again, the observed discontinuity in the melting rate is consistent with the formation of a protective ice crust on melting octane when $T_\infty < 13$°C. Recall that the present crust/melt layer model predicts the onset of crust formation to be independent of jet velocity [see Equation (36)]. Moreover, calculations indicate that for water jet impingement on melting octane, incipient ice crust formation is predicted when the jet temperature drops below 15°C; this prediction is in excellent agreement with the temperature at which the step change in melting rate is observed.

When the water jet temperature was reduced below about 5°C, the ice crust was sufficiently thick to be observed visually. The crust was observed to be quite stationary; it did not meander about owing to disturbances in the jet. Alternate growth and remelting of the crust, found in simultaneous melting and freezing in a pipe flow (Yim et al., 1978), was not observed. Also, melted material could be seen flowing out from between the ice crust and the melting surface. This was quite apparent for the case of melting mercury which, because of its bright silver color, contrasts greatly with the clear ice crust. The mercury flowed over the radial edge of the ice crust and was swept away by the deflected water jet. Photographing the ice crust in place on the melting surface was hampered by the presence of the deflected fan jet. High speed framing camera photography produced the photograph shown in Figure 5 of the ice crust during free fall immediately after the jet was shut off.

At the condition of incipient crust formation, $T_\infty \cong 13$°C, an interesting octane rod melting behavior was observed and recorded on the rod displacement/time chart displayed in Figure 6. The rod moves slowly with time at first, revealing a melting velocity that lies on the lower curve in Figure 4 at 13°C. After about 23 s into the run, the melting velocity suddenly increases

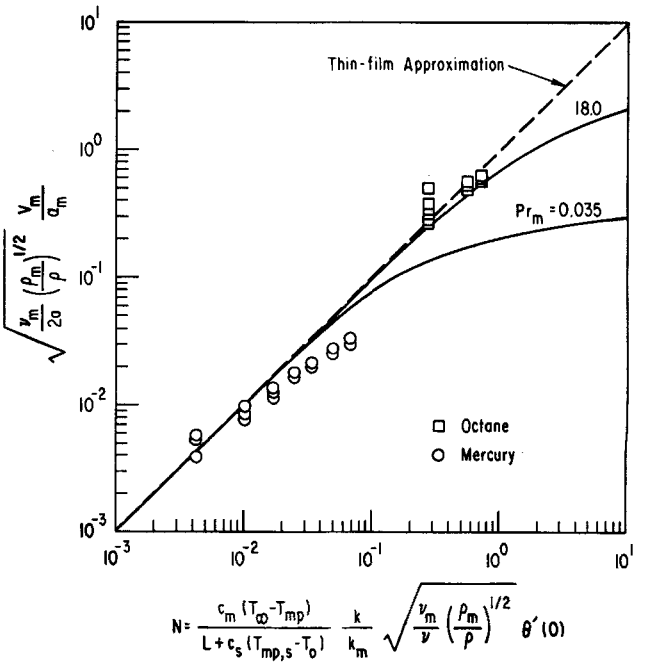

Figure 8. Melting rate of an octane rod and a mercury rod; comparison of theory and experiment. Thin film approximation Equation (34) - - -; exact (numerical) solution of Equations (17) and (18) ———.

* Strictly speaking, the melting velocity is not identically zero at $T_\infty = 0$°C. In this limit, heat transfer is due to pure transient conduction and $V_m \sim (\alpha_s/t)^{1/2}$.

to a higher value, which corresponds with data points on the upper curve in Figure 4. This is followed by two more step changes in melting velocity of identical magnitude before the octane rod melting process is complete. This would seem to indicate that, at incipient crusting, the ultrathin ice layers that form are unstable against slight perturbations in jet temperature. More important, it is clear that the formation of a stationary crust, no matter how thin, effects an abrupt change in the motion and convection within the jet, which causes a sudden reduction in the rod melting rate.

The melting rate data for water jet impingement on melting mercury are shown in Figure 7. Qualitatively, the melting behavior is similar to that of octane at low jet temperatures insofar as the melting velocity decreases with decreasing T_∞, approaching zero when $T_\infty \to 0$°C, illustrating once again the thermally protective nature of the ice crust. The one obvious distinction between the melting rate data for the octane rod and for the mercury rod is that over the jet temperature range investigated, the melting mercury rod does not appear to lose its protective ice cover. The results of calculations using Equation (36) show that incipient crust formation will occur at a water jet temperature equal to 117°C; consequently, for the range of jet temperatures studied here, an ice crust will always be present on melting mercury. This explains the absence of a temperature threshold or melting rate discontinuity in Figure 7. Also shown in Figure 7 is the result of calculations of V_m based on a two material axisymmetric flow model that accurately predicts melting rates in situations in which the impinging liquid does not freeze on the melting solid (Swedish et al., 1979). The no-crust melting theory is seen to overestimate the mercury melting rate by about one order of magnitude for $0 < T_\infty < 10$°C; it is found to overestimate V_m by a factor of 4.0 for T_∞ as high as 80°C.

In Figure 8, the experimental melting rates are compared with the numerical solutions (dark curves) as well as with the thin melt film approximation (dashed curve). The approximate solution, Equation (34), and the numerical solutions which include the effects of melt film inertia and convection agree quite well over the range of water jet temperatures used in the experimental investigation.

There is good agreement between the trends of the data and the predicted values. However, for the highest jet temperatures, the predicted mercury melting rates are about 60% above measurements. This discrepancy is probably due to the effects of the initial subcooling of the mercury rod which was difficult to control at higher jet temperatures. As already mentioned, the mercury rod was enclosed within a lucite container for safety purposes. Heating of the air in the container by the apparatus caused the rod to experience a relatively rapid temperature rise during the experiment and melt prematurely along its entire length. In order to compensate for this, the initial rod subcooling was increased (that is, a shorter preheating period was used).

It is interesting to note that the presented theory predicts that a jet of molten ceramic UO_2 must be heated above 9 400°C before it fails to solidify as a crust on melting steel.

ACKNOWLEDGMENT

The authors wish to express their sincere thanks to Kathy Cummings for the typing of the manuscript.

This work was performed under the auspices of the U.S. Department of Energy.

NOTATION

a = stagnation point velocity gradient, w_∞/d
A = dimensionless property ratio, Equation (24)
a_m = stagnation point velocity gradient for melt film, Equation (15)
B = dimensionless property ratio, Equation (24)
c = heat capacity
d = diameter of nozzle orifice
f = dimensionless similarity velocity variable
F = dimensionless similarity pressure variable
k = thermal conductivity
L = latent heat of fusion of the melting solid material
N = melting parameter, Equation (23)
p = pressure in melt layer
P = pressure in jet flow at the crust surface
p_0 = pressure at stagnation point
Pr = Prandtl number
q = heat flux through crust
r = radial coordinate
R = radius of crust disk
T = temperature
T_i = temperature at crust melt film interface
T_{mp} = melting point of the jet material
$T_{mp,s}$ = melting point of the solid material
T_0 = temperature in the solid at a large distance from the melting surface
$T_{\infty,crit}$ = jet temperature above which crust formation will not occur
u = velocity component in r direction
V_m = melting velocity
w = velocity component in z direction
z = transverse coordinate measured from melting surface

Greek Letters

α = thermal diffusivity
δ = melt film thickness
δ_c = crust thickness
η = dimensionless similarity coordinate, Equation (14)
η_δ = dimensionless melt film thickness, $\delta(2a_m/\nu_m)^{\frac{1}{2}}$
$\theta'(0)$ = dimensionless temperature gradient, Equation (1)
μ = absolute viscosity
ν = kinematic viscosity
ρ = density
ϕ = dimensionless temperature in the melt layer, Equation (16)

Subscripts

c = crust
m = melt film
s = solid
∞ = at the nozzle orifice or edge of boundary layer in the jet flow

LITERATURE CITED

Carslaw, H. S., and J. C., Jaeger, *Conduction of Heat in Solids*, 2 ed., p. 292, Oxford University Press, England (1959).

Charles, G. E., and S. G. Mason, "The Coalescence of Liquid Drops with Flat Liquid/Liquid Interfaces," *J. Colloid Sci.*, **15**, 236 (1960).

Donaldson, C. D., R. S. Snedeker and D. P. Margolis, "A Study of Free Jet Impingement, Part 2. Free Jet Turbulent Structure and Impingement Heat Transfer," *J. Fluid Mech.*, **45**, 477 (1971).

Epstein, M., "Stability of a Submerged Frozen Crust," *Trans. ASME J. Heat Transfer*, **99**, 527 (1977).

———., M. J. Swedish, J. H. Linehan, G. A. Lambert, G. M. Hauser and L. J. Stachyra, "Heat Transfer and Fluid Dynamics," in Reactor Development Program Progress Report, ANL-RDP-68, Argonne National Laboratory, p. 6.56 (Feb., 1978).

Erickson, G. G., and D. B. Olfe, "Growth and Decay of Perturbations at an Interface in a Stagnation Counterflow," *J. Fluid Mech.*, **84**, 401 (1978).

Gilpin, R. R., "The Ablation of Ice by a Water Jet," *Trans. Can. Soc. Mech. Engrs.*, **2**, 91 (1973).

Giralt, F., C. J. Chia and O. Trauss, "Characterization of the Impingement Region in an Axisymmetric Turbulent Jet," *Ind. Eng. Chem. Fundamentals*, **16**, 21 (1977).

Lipsett, A. W., and R. R. Gilpin, "Laminar Jet Impingement Heat Transfer Including the Effects of Melting," *Int. J. Heat Mass Transfer*, **21**, 25 (1978).

Martin, H., "Heat and Mass Transfer between Impinging Gas Jets and Solid Surfaces," *Advances in Heat Transfer*, Vol. 3, p. 1, Academic Press, New York (1977).

Roberts, A. L., "On the Melting of a Semi-Infinite Body Placed in a Warm Stream of Air," *J. Fluid Mech.*, 4, 505 (1958).
Savino, J. M., J. F. Zumdieck and R. Siegel, "Experimental Study of Freezing and Melting of Flowing Warm Water at a Stagnation Point on a Cold Plate," Fourth Int. Heat Transfer Conference, Paris-Versailles, 1, Cu 2.10 (1970).
Schlichting, H., *Boundary Layer Theory*, p. 83, McGraw-Hill, New York (1960).
Sitharamayya, S., and K. Subba Raju, "Heat Transfer Between an Axisymmetric Jet and a Plate Held Normal to the Flow," *Can. J. Chem. Eng.*, 47, 365 (1969).
Stewart, W. E., and R. Prober, "Heat Transfer and Diffusion in Wedge Flows with Rapid Mass Transfer," *Int. J. Heat Mass Transfer*, 5, 1149 (1962).
Swedish, M. J., M. Epstein, J. H. Linehan, G. A. Lambert, G. M. Hauser and L. J. Stachyra, "Surface Ablation in the Impingement Region of a Liquid Jet," *AIChE J.*, 25, 630 (1979).
Yang, K. T., "Formation of Ice in Plant Stagnation Flow," *Appl. Sci. Res.*, 17, 377 (1966).
Yim, A., M. Epstein, S. G. Bankoff, G. A. Lambert and G. M. Hauser, "Freezing-Melting Heat Transfer in a Tube Flow," *Int. J. Heat Mass Transfer*, 21, 1185 (1978).
Yen, Y. C., and A. Zehnder, "Melting Heat Transfer with Water Jet," *ibid.*, 16, 219 (1973).
Yen, Y. C., "Heat-Transfer Characteristics of a Bubble-Induced Water Jet Impinging on an Ice Surface," *ibid.*, 18, 917 (1975).

Manuscript received March 12, 1979; revision received February 12, and accepted February 29, 1980.

Viscous Heat Generation in Slit Flow

The onset of significant departure from isothermality caused by viscous energy dissipation in flow through a slit is determined for isothermal and adiabatic walls. A series solution of the energy equation enables calculation of dimensionless profiles for any power law fluid. Such solutions provide useful standards for judging performances of numerical schemes for solving complex nonisothermal flows.

ROBERT M. YBARRA
and
ROGER E. ECKERT
School of Chemical Engineering
Purdue University
West Lafayette, Indiana 47907

SCOPE

When a viscous fluid in a slit is set in flow by a large imposed pressure gradient, a vast amount of mechanical energy is converted irreversibly into heat owing to the fluid's internal friction. This viscous heat dissipation not only leads to an overall increase in the fluid's bulk temperature but also causes a noticeable temperature variation to develop across the shear field. Significant viscous heating occurs when the heat generated by the shearing of adjacent fluid layers is on the order of the heat which is removed by conduction through a slit wall. Since rheological properties, such as viscosity, are strongly temperature dependent, any rheological measurement not conducted under completely isothermal conditions can be erroneous and the observed fluid behavior misleading. In fact, heat effects can induce an apparent non-Newtonian behavior in Newtonian fluids.

The apparent nonlinear behavior which is exhibited by a general fluid undergoing deformation may be the result of two different mechanisms. The first is the dependence of the rheological properties on the fluid's state of deformation. This mechanism has been the major concern of most of the research in non-Newtonian fluid mechanics. The second mechanism is the dependence of the rheological properties on the thermodynamic state of the fluid, that is, the temperature and pressure. Since most fluids are relatively incompressible, except at extremely high pressures, the effect of pressure on the rheological behavior is neglected in this work. Variation in temperature due to shearing and resultant heat transfer in flow through a slit is treated.

The parallel plate geometry plays a significant part in such polymer processing operations as extrusion of thin film and flow of molten polymer through the shallow channel of a screw pump. Furthermore, experimental investigations (Novotny and Eckert, 1973, 1974) have clearly established that the slit geometry is an advantageous means of accurately determining rheological properties of viscoelastic liquids in the high shear flow regime, a region where most macromolecular fluids are processed. However, the use of the slit as a rheological geometry is not widespread. Moreover, the study of the nonisothermal slit flow of non-Newtonian fluids has received relatively little attention despite the industrial and scientific importance of this geometry.

Laminar heat transfer of a non-Newtonian fluid in slit flow but without viscous heat generation has been dealt with by several authors (Tien, 1962; Suckow et al., 1971; Kwant and Van Ravenstein, 1973). The first two authors developed solutions to the slit's analogue of the Graetz-Nusselt problem for power law fluids, whereas Kwant and Van Ravenstein studied the heat transfer rate and the effect of this transfer upon the hydrodynamics for power law fluids.

At the high shear rates normally used to process macromolecular fluids in parallel plate channels, considerable heat is generated, but this topic has been treated by relatively few investigators. Seifert (1969) calculated the developing temperature profile for a Prandtl-Eyring fluid with emphasis on the heat flux at the slit wall for symmetric and asymmetric wall temperatures. Vlachopoulos and Keung (1972) numerically solved the energy equation for a power law fluid in fully developed flow and presented the results in terms of the Nusselt number and bulk temperature rise. Cox and Macosko (1974) experimentally investigated the surface temperature rise of poly(acrylonitrile cobutadiene-styrene) (ABS) and polyethylene (PE) extruded through slits and associated geometries using an infrared pyrometer. For fluids with variable density and shear and temperature dependent viscosity, they numerically treat the mass, momentum and energy equations. Winter (1975, 1977) treated the viscous dissipation problem for a power law fluid whose viscosity decreases exponentially with temperature using an implicit iterative numerical scheme for the solution of the equations of change.

In the present work, analytical solutions are obtained for the problem of viscous generation for non-Newtonian fluids in slit flow. Both isothermal and adiabatic slit wall cases are treated. The fluids studied are assumed to be adequately described by a power law shear stress dependence. Since our ultimate goal is